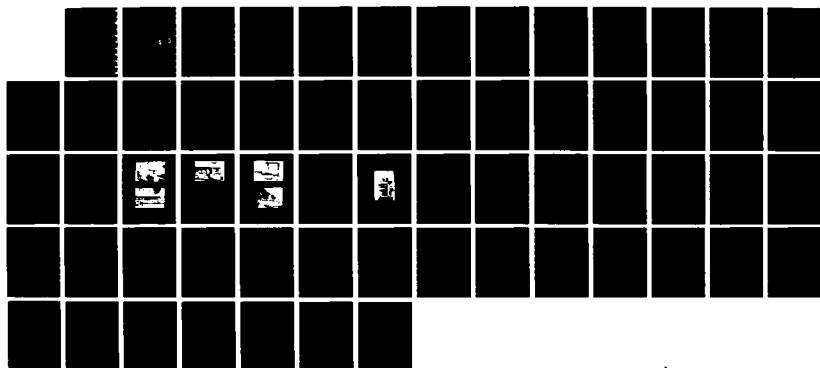AD-A178 854   OPTICAL DEPOLARIZATION OF THIN METAL FILMS(U) AIR FORCE   1/1
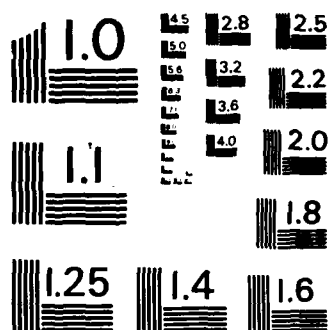   INST OF TECH WRIGHT-PATTERSON AFB OH J D HOEFT APR 86
               AFIT/CI/NR-86-92T

UNCLASSIFIED   F/G 14/2   NL

MICROCOPY RESOLUTION TEST CHART

NATIONAL BUREAU OF STANDARDS-1963-A

REPORT DOCUMENTATION PAGE		READ INSTRUCTIONS BEFORE COMPLETING FORM
1. REPORT NUMBER AFIT/CI/NR 86-92T	2. GOVT ACCESSION NO.	3. RECIPIENT'S CATALOG NUMBER
4. TITLE (and Subtitle) Optical Depolarization Of Thin Metal Films		5. TYPE OF REPORT & PERIOD COVERED THESIS/DISSERTATION
		6. PERFORMING ORG. REPORT NUMBER
7. AUTHOR(s) John David Hoeft		8. CONTRACT OR GRANT NUMBER(s)
PERFORMING ORGANIZATION NAME AND ADDRESS AFIT STUDENT AT: University of New Mexico		10. PROGRAM ELEMENT, PROJECT, TASK AREA & WORK UNIT NUMBERS
CONTROLLING OFFICE NAME AND ADDRESS AFIT/NR WPAFB OH 45433-6583		12. REPORT DATE 1986
		13. NUMBER OF PAGES 49
MONITORING AGENCY NAME & ADDRESS(If different from Controlling Office)		15. SECURITY CLASS. (of this report) UNCLAS
		15a. DECLASSIFICATION/DOWNGRADING SCHEDULE

DISTRIBUTION STATEMENT (of this Report)

APPROVED FOR PUBLIC RELEASE; DISTRIBUTION UNLIMITED

DTIC
ELECTE
AUG 1 3 1986
S E D

17. DISTRIBUTION STATEMENT (of the abstract entered in Block 20, if different from Report)

18. SUPPLEMENTARY NOTES

APPROVED FOR PUBLIC RELEASE: IAW AFR 190-1

LYNN E. WOLAVER 6 AUG 86
Dean for Research and
Professional Development
AFIT/NR

19. KEY WORDS (Continue on reverse side if necessary and identify by block number)

20. ABSTRACT (Continue on reverse side if necessary and identify by block number)

ATTACHED.

DD FORM 1473 EDITION OF 1 NOV 65 IS OBSOLETE
1 JAN 73

86 5 12 024

AD-A170 854

DTIC FILE COPY

ACKNOWLEDGMENTS

I would like to thank J.R. McNeil, G.A. Al-Jumaily, and J.J. McNally for their help in completing this masters degree. I would also like to acknowledge the rest of the Thin Films laboratory at the University of New Mexico Electrical Engineering Department for their invaluable help.

iii

OPTICAL DEPOLARIZATION OF THIN METAL FILMS

By

JOHN DAVID HOEFT

ABSTRACT OF THESIS

Submitted in Partial Fulfillment of the
Requirements for the Degree of

Master of Science in Electrical Engineering
The University of New Mexico
Albuquerque, New Mexico

April, 1986

OPTICAL DEPOLARIZATION OF THIN METAL FILMS

John David Hoeft

B.S. Electrical Engineering,
New Mexico State University 1984

M.S. Electrical Engineering/Optical Engineering,
University of New Mexico 1986

All optical surfaces exhibit some degree of roughness. As a consequence of this, some of the scattered light is depolarized. Depolarization of scattered light has been previously investigated in connection with radar theory.(1) This study examined depolarization of scattered light from thin metal films using an angle-resolved optical scatterometer. The effect of varying surface morphology on the intensity of the depolarized light was investigated. The results establish that in the smooth surface limit, depolarization has little dependence on surface roughness. The intensity of depolarized light increased for surfaces which have relatively more high frequency microroughness.

TABLE OF CONTENTS

LIST OF FIGURES

LIST OF TABLES

x

LIST OF PLATES

1. INTRODUCTION

Optical surfaces have some scatter associated with
them regardless of how well they are prepared. First
order vector scatter theory describes the behavior of
scattered light intensity as a function of geometry and
surface parameters. However, this theory does not predict
optical depolarization in the plane of incidence. It is
necessary to use second order vector scatter theory to
predict this. The purpose of this study is to extend the
scope of the research that has been done on optical
depolarization of thin metal films.

1.1   Description of problem

The major thrust of this study was to gather data on
depolarization of light intensity in the plane of
incidence so that vector scatter theory could be
evaluated. Measurenents were made so that the results
could be used for the following reasons:

> To verify that our calculations based upon vector
> scatter theory of optical radiation are accurate,
>
> To study how different angles of incidence influence
> the depolarization of optical scatter from optical
> surfaces,
>
> To determine how surface morphology affects the
> depolarization of optical scatter from surfaces, and

To compare our results of depolarization measurements to (limited) results of other investigators, within the scope of our capability.

1.2   Literature review

Depolarization of waves reflected from a surface was first investigated by Barrick (1) who modeled the backscatter of radar signals using first order theory. Barrick established relationships between backscatter intensity and surface roughness in terms of the radar cross section per unit area.

Barrick's results led Church (2) to explore backscatter at optical wavelengths. Church defined the relationship between differential scatter elements and incident light intensity. He also limited his area of analysis to nonmagnetic and highly conducting surfaces. These limitations allowed him to develop a relation for intensity ratio of scattered light (Is) over incident light (Ii) that could be integrated over the front hemisphere of the surface, thus allowing the surface roughness to be calculated. In addition, this relation includes a term that represents the power spectral density. The power spectral density (PSD) function is the square magnitude of the two-dimensional Fourier transform of the surface height function. The RMS roughness is defined to be the integration of the PSD function over a

2

specified spatial frequency bandwidth.

Stover (3) extended Church's results to incorporate
measurable quantities, such as angles of incidence (θi)
and scatter (θs), aperture width (Ω), scattered light
intensity (Is), incident light intensity (Ii), and
incident light wavelength (τ).   In this study, Stover's
theory has been used to find the PSD and RMS surface
roughness of optical thin films.   These are summarized in
chapter 2.

Depolarization of scattered light has been
investigated theoretically by several authors.   Valenzuela
(4) used Rice's (5) theory to obtain depolarization from
slightly rough surfaces in the plane of incidence.   This
was achieved using second order vector scatter theory,
which takes into account multiple reflections.   Second
order scatter theory is beyond the scope of this study.

Depolarization in the plane of incidence was measured
by Jansen (6) and Bennett (7).   Jansen measured
depolarization from copper thin films for a single angle
of scatter.   Bennett measured the retroscatter from silver
and aluminum thin films.   Retroscatter is the scattered
light that reflects back to the incident beam from the
sample.

Measurements for this study were made using Stovers method. The depolarization measurements were similar to those made by Bennett and Jansen. But in this study measurements were made in a continuous fashion across the entire front plane of incidence instead of at several discrete points.

Vector scatter theory is reviewed in Chapter 2. Chapter 3, is a description of the experimental arrangement. A description of the data collection methods is in Chapter 4. In Chapter 5, the results of the study are presented. In Chapter 6, the results are discussed. In Chapter 7, conclusions and suggested areas of future studies are made.

2. THEORETICAL BACKGROUND

In order to insure the calculation of the power spectral density (PSD) was being correctly performed, it was necessary to examine the development of vector scatter theory. Once this background was obtained, the performance of the scatterometer could be more fully examined.

2.1 Description of Power Spectral Density

The PSD of optical surfaces is derived from first order vector scatter theory. Vector scatter theory is based on the assumption that the surface RMS roughness is much smaller than the wavelength of the incident light. There are two approximate solutions to the problem of scattering from smooth surfaces. One approach is to use the Kirchoff integrals, which in principal give exact answers but several assumptions must be made to solve the integrals. The second is by making small perturbations to an ideal surface. It is this second method that will be followed here.

The relationship between scattering and surface topology has been studied in regard to radar backscatter. (8) This relationship is usually complicated, but in the smooth surface limit the connection becomes simple. Two

researchers have pioneered the application of vector diffraction theories for optical scatter, Church (9) and Elson. (10) Church's treatment will be followed in relating the scattered light to surface roughness.

Vector scattering functions have the form

$$\frac{1}{Ii} \frac{dIs}{\Omega} = \frac{C}{\tau^4} \; Qi(\Theta i, \; \Theta s, \; \breve{\Phi}i, \; \breve{\Phi}s, \; n, \; x_o, \; y_o) \; W(p,q).$$

2.1 1

where C is a constant, τ is the wavelength, n is the complex index of refraction, Θi and $\breve{\Phi}i$ are incident angles and Θs and $\breve{\Phi}s$ are scattered angles. Figure 2.1 depicts the angles that are used in equation 2.1 1. The scattering intensity is inversely proportional to the fourth power of wavelength (τ), as in Rayleigh or Mie scattering. The quantity Qi is the optical factor, which is independent of conditions of surface and depends on the geometry of the scatter calculation. The surface factor W(p,q) is the PSD of the surface roughness. The relationship between the differential scattered light intensity and the PSD of the surface roughness is given by

$$\frac{1}{Ii} \frac{dIs}{\Omega} \Omega = 4 \; ko^4 \; cos\Theta i \; cos^2\Theta s \; Q[\tau\delta] \; W(p,q) \; \Omega \; .$$

2.1 2

where Ω is the solid angle of the detection system, ko equals $2\pi/\tau$ is the wavenumber, and $Q[\tau\delta]$ is the Q factor discussed in section 2.3.

6

Measurement of scattered light provides a method of finding the PSD. Equation 2.1 2 can be considered as the first term in the vector perturbation expansion in terms of the parameter $(k_0\sigma)^2$, where σ is the RMS roughness. This theory relates the scattered light intensity as a function of angle. It does not predict depolarization in the plane of incidence. Depolarization in the plane of incidence is a second order effect, and more terms must be included for the theory to predict depolarization. By rearranging equation 2.1 2, a function for the PSD can be given by

$$W(p,q) = \frac{(I_s/I_i \; (dI/\Omega))}{(4k_0^4 \cos\theta_i \cos^2\theta_s \; Q)}. \qquad 2.1 \; 3$$

Stover (3) modified this relationship to be in terms of measurable quantities, such as incident and scatter angle, incident and scatter light intensities, to be

$$W_{1/2}(\theta_i,\theta_s) = \frac{(I_s/I_i \; 1\times10^8 \; \tau^3)}{(8\pi^2 \cos\theta_i \cos^2\theta_s \; \Omega \; Q[\tau\delta])} . \qquad 2.1 \; 4$$

If the wavelength is measured in microns and roughness in Angstroms, then the units of the PSD are Angstroms^2 per micron^{-2}

2.2 Calculation of RMS surface roughness

The RMS roughness is calculated by integrating the PSD function over a specified spatial frequency bandwidth.

The RMS surface roughness is given by

$$RMS = [\int \int W(f_x, f_y) \, df_x \, df_y]^{1/2} \qquad . \qquad 2.2\ 1$$

2.3   The Q factor

The Q factor in equation 2.1 2 contains the dependence of the scattered light on the state of polarization of the incident (Γ) and scattered (δ) light. The polarizations Γ and δ are either S or P polarization. S polarization is light where the E field is orientated 90° out of the plane of incidence. P polarization is light where the E field is orientated in the plane of incidence.   It also contains factors for the measurement geometry and the optical constants of the surface.   The four factors are given by:

$$Q[SS] = [\frac{(\epsilon-1)\cos\delta s}{[\cos\theta i + (\epsilon - \sin^2\theta i)^{1/2}][\cos\theta s + (\epsilon - \sin^2\theta s)^{1/2}]}]^2 , \qquad 2.3\ 1$$

$$Q[SP] = [\frac{(\epsilon-1)\sin\delta s \ (\epsilon - \sin^2\theta s)^{1/2}}{[\cos\theta i + (\epsilon - \sin^2\theta i)^{1/2}][\epsilon\cos\theta s + (\epsilon - \sin^2\theta s)^{1/2}]}]^2 , \qquad 2.3\ 2$$

$$Q[PS] = [\frac{(\epsilon-1)\sin\delta s \ (\epsilon - \sin^2\theta i)^{1/2}}{[\epsilon\cos\theta i + (\epsilon - \sin^2\theta i)^{1/2}][\cos\theta s + (\epsilon - \sin^2\theta s)^{1/2}]}]^2 , \qquad 2.3\ 3$$

$$Q[PP] = [\frac{(\epsilon-1)(\epsilon - \sin^2\theta i)^{1/2} (\epsilon - \sin^2\theta s)^{1/2}\cos\delta s - \epsilon\sin\theta i \ \sin\theta s}{[\epsilon\cos\theta i + (\epsilon - \sin^2\theta i)^{1/2}][\cos\theta s + (\epsilon - \sin^2\theta s)^{1/2}]}]^2 . \qquad 2.3\ 4$$

Where the first subscript is the incident light

polarization and the second is the collected scattered
light polarization. Using these expressions, in the plane
of incidence where $\phi s = 0°$, the Q factor equals zero for
cross polarized measurements. In the limit of small
scattering angles $\theta s = \theta i$, the Q factor reduces to the
reflectance (R[S]) of the surface.
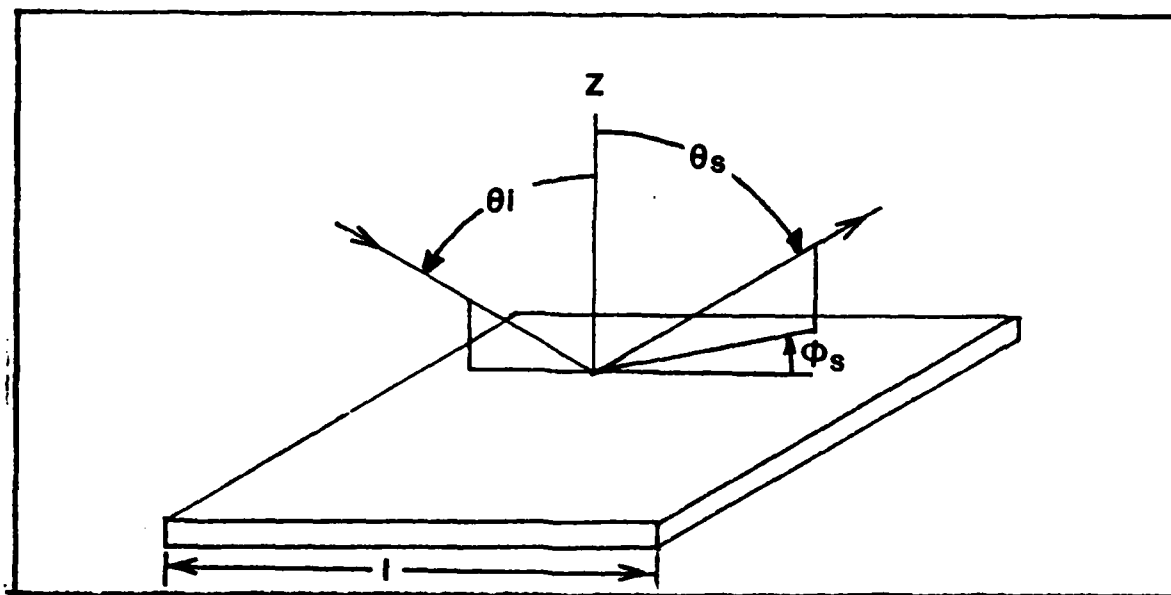
Figure 2.1 Definition of all angles pertinent to the calculation.

I.   EXPERIMENTAL ARRANGEMENT

Over the last few years, the angle-resolved optical
scatterometer at the University of New Mexico Thin Films
Laboratory has been continuously upgraded to incorporate
new areas of research. The original system consisted of
an HeNe laser as a light source, an optical system
consisting of spatial filters and lenses to remove higher
diffraction orders and focus the beam, and a detection
system consisting of a photo multiplier tube (PMT) and a
rotating table. The entire system was enclosed in a
darkened part of a clean room so that background light
would not affect measurements. This system could measure
optical scatter in both transmissive and reflective
optical components. It could measure scattered radiation
from optical components at near normal incidence, and
throughout one half of the plane of incidence.

For this study, it was necessary to make several
upgrades. The scatterometer, after the improvements, is
shown in plate 3.1. These improvements and the increased
capabilities are listed below:

    Implementing a position encoder to allow more
    accuracy in measuring the angular position of the
    detector;

    Installing an argon ion laser to permit
    multi-wavelength scatter measurements;

Implementing new computer programs for improved data
collection and increased flexibility in analysis of
the raw data;

Implementing polarization measurement capabilities;

Installing a new analog-to-digital converter (ADC)
to provide more precise measurements of the scattered
light intensities.

3.1   Lasers

Two lasers, an argon ion and an helium neon, provide

light for the optical system, see plate 3.2.   The HeNe

laser is a 15 mw continuous wave (CW) laser operating at

633 nm.   The argon ion laser is a variable power CW laser

with a maximum power of 7 w, capable of operating at 350,

488 and 514 nm.   Both of the lasers are polarized in the S

direction.   This flexibility in power and wavelength

allows the measurement of dielectric films at half and

full wave optical thicknesses, and permits the measurement

of optical components with lower reflectance.

3.2   Optical system

The optical system consists of a spatial filter,

apertures, and lenses.   The output from the lasers passes

through the optical system and is focused onto the

detector.   The system configuration is shown in plate 3.2,

3.3, and in figure 3.1.   In this improved system, the

polarized beam emitted from the laser passes through a

half wave plate which rotates the beam polarization to the
desired direction. The beam is passed through a polarizer
to reject the undesired polarization. This beam is turned
by two beam steering mirrors; these align the beam across
the center of the detection system. The aligned beam
passes through another polarizer to increase the rejection
ratio. The beam is chopped so that a heterodyne detection
system can be used to measure the light intensity. The
beam can pass through a set of neutral density filters
that reduce the beam intensity and thus allow the specular
beam to be measured. The beam is then passed through a
spatial filter which removes all spatial frequencies
except for the central order. The beam is focused on the
detector collecting lens using a high-quality, low-scatter
focusing lens. This is done so the measurements are made
in the far field. To terminate any stray light from the
focusing lens, the focused beam is passed through several
apertures. Another polarizer is placed in front of the
detector. The direction of this polarizer can be
orientated to measure light of the same polarization as
the input or to measure the cross polarized signal. This
arrangement including multiple polarizers yields a
polarization rejection ratio of 10000:1. When
polarization measurements are not being made, the
polarizers and the half wave plate are removed from the
system.

3.3   Detection system

The detection system shown in plate 3.4 is used for measuring the intensity of scattered light as a function of angle.   Although it can measure optical scatter either in transmission or reflection, in this work the instrument was only used in reflectance.   The detection system consists of a rotatable table on top of a stable surface. A fiber optic and PMT are mounted on the table and can be rotated over 270°.   A sample mount with five degrees of freedom is used to hold coating samples.   The table position is monitored by the computer through an optical position encoder.   The resolution of the encoder is .015 ± .007 degrees per count, which allows for a precise measurement of table position relative to the specular beam.   All of the measurements are made in the same direction to reduce position errors.   The intensity of the scattered light is monitored by the computer through a lock-in amplifier and an ADC.

The light reflected from the sample passes through the final polarizer and is collected by the lens and is passed to the detector.   See plate 3.5.   This arrangement has a collecting lens, a field stop and a fiber optic. Figure 3.2 illustrates the geometry of the fiber optic collection system.   The lens focal length is 16 mm

and the lens diameter is 4 mm. The image of the fiber
optic is larger than the image of the field stop. The
lens of figure 3.2 is the aperture stop of the system: the
detector solid angle (Ω) is limited by the aperture stop
to .00011 steradians (sr). From figure 3.2, it can be
seen that all rays originating from a circle of diameter $\emptyset$
enter the fiber and are detected. Using the dimensions of
figure 3.2, $\emptyset = 7.5$ mm. The illuminated spot on the
sample is 2.0 mm diameter and is within this 7.5 mm
diameter area. The field of view of the system is limited
by the field stop to a collection area of 17.6 mm diameter
on the sample. This arrangement also reduces the
influence of vibrations in the measurements.

By assuming that the light is approximately a plane
wave at the optic a minimum sampling interval can be
found. A minimum sampling interval is found by
considering the angle subtended by the detector collecting
lens (aperture stop). This angle is the amount that the
detector would have to be moved if the detector were not
to measure the same scattered light more than once. From
the dimensions in figure 3.2 this angle is .68°. Because
the measurements are made with smaller sampling intervals
than .68° the data is averaged in a manner that warrants
discussion. The angle subtended by the detector relates
to a bandwidth of spatial frequencies for each data

15

point. Therefore each data point on a PSD curve
corresponds to averaging the scattered light over a
bandwidth of spatial frequencies, which will be called
Spatial Frequency Width (SFW). This width is dependent on
the scatter angle and is given by

$$SFW = Fmax - Fmin \qquad\qquad 3.3\ 1$$

$$SFW = \frac{\sin(\theta s+.34°)-\sin(\theta i)}{r} - \frac{\sin(\theta s-.34°)-\sin(\theta i)}{r}. \qquad 3.3\ 2$$

The maximum value of the SFW occurs for a frequency of 0.
microns^{-1} which corresponds to $\theta s = 0°$ and is 0.0137
microns^{-1}. In measurements of RMS roughness, the
largest angle used is 70°, this corresponds to a spatial
frequency of 1.485 microns^{-1}, and a SFW of .0064
microns^{-1}. To decrease the SFW of each measurement
point it is necessary to reduce the size of the detector
collecting lens.

One method of determining the sensitivity of the
system is to determine the minimum detectable BRDF of the
system. This is set by the the dark current of the
system, and is 6.6×10^{-8} sr^{-1}. The maximum BRDF
scatter is the inverse of the solid angle of detection (Ω)
and is 9091. sr^{-1}. To measure a sample with the maximum
sensitivity (which corresponds to the minimum BRDF), it is
necessary to reduce the sampling rate by an order of
magnitude of what is normally used. This is necessary in

16

order to accommodate increase in the time constant of the measurement apparatus. Including this, the dynamic range of the system is eleven orders of magnitude (1.37×10^{11}). Another method to characterize the sensitivity of the scatterometer system is to consider the equivalent system RMS roughness. This is found by measuring the scatter from the incident laser beam and analyzing this to find the equivalent system RMS roughness. The equivalent system RMS roughness is measured every time the scatterometer is used and is typically less than 3.0 Angstroms, as measured within the spatial frequency bandwidth of the system ($.014$ microns^{-1} to 1.6 microns^{-1}).

The light that reaches the end of the fiber optic is dispersed by a piece of ground glass to ensure that a direct beam of light does not reach the PMT. See figure 3.3. The beam passes through an interference filter centered at the wavelength of interest to minimize any problems caused by stray light. A resistor converts the PMT current into a voltage, and this is measured by a lock-in amplifier. This amplifier has ranges from 100 mV to 1 μV full scale, which corresponds to 10 μA to 100 pA. Because the dark current of the PMT is approximately 2 pA in the 1 Hz bandwidth of the lock-in, the 1 μV range is not normally used.

17

The lock-in amplifier output, zero to ten volts, is applied to the ADC of the computer. All the position and intensity measurements are recorded directly by the computer. This technique not only reduces the difficulty of making measurements, but it also provides better records and removes some of the art of making measurements.

3.4   Computer interfaces

The computer used to make these measurements is a Digital LSI-11/03; see plate 3.6. Although another computer, the LSI-11/23, was used for software development, the software runs on either machine. The computer uses a menu-driven control program listed in Appendix 1 that provides more flexibility in measurement techniques. The sensors on the detection system give the computer information about the position of the detector and the intensity of the light signal. The computer continuously monitors the position of the detector and the intensity of the light.
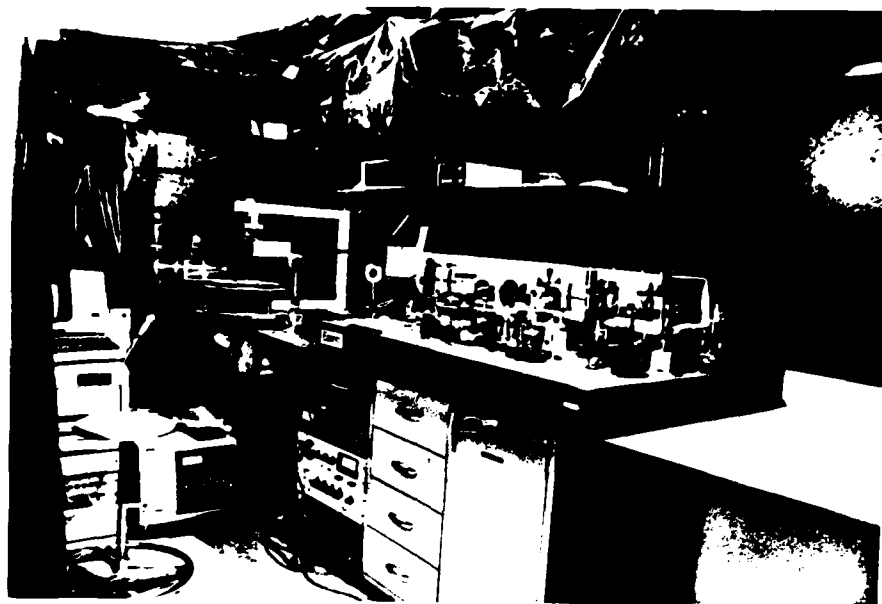
Plate 3.1 The scatterometer system.
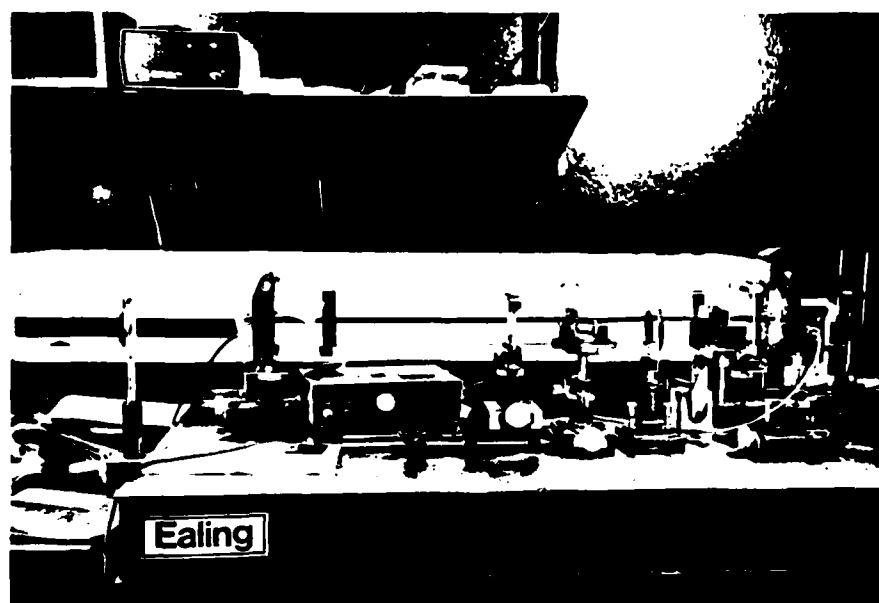
Plate 3.2 Argon and HeNe laser at start of optical
system.
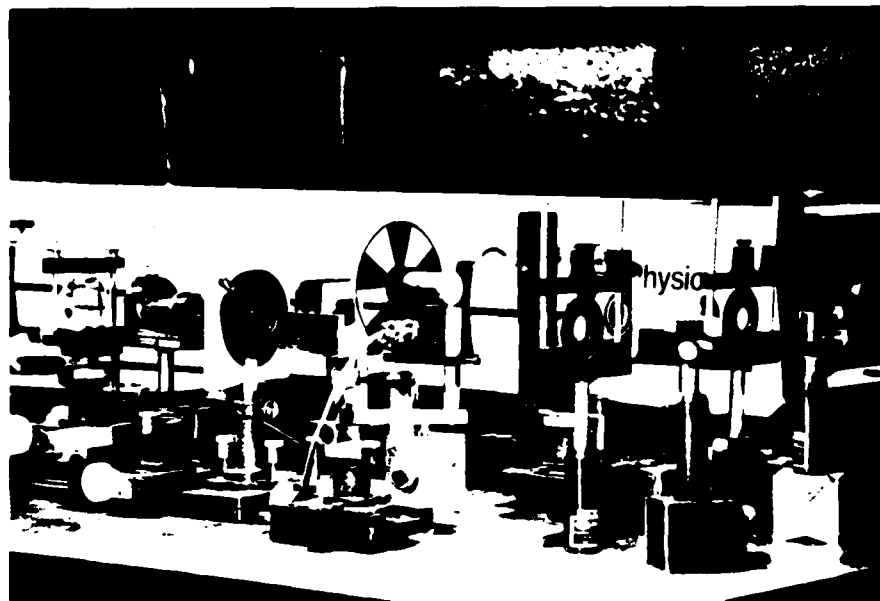
Plate 3.3 Optical system from lasers to scatterometer.
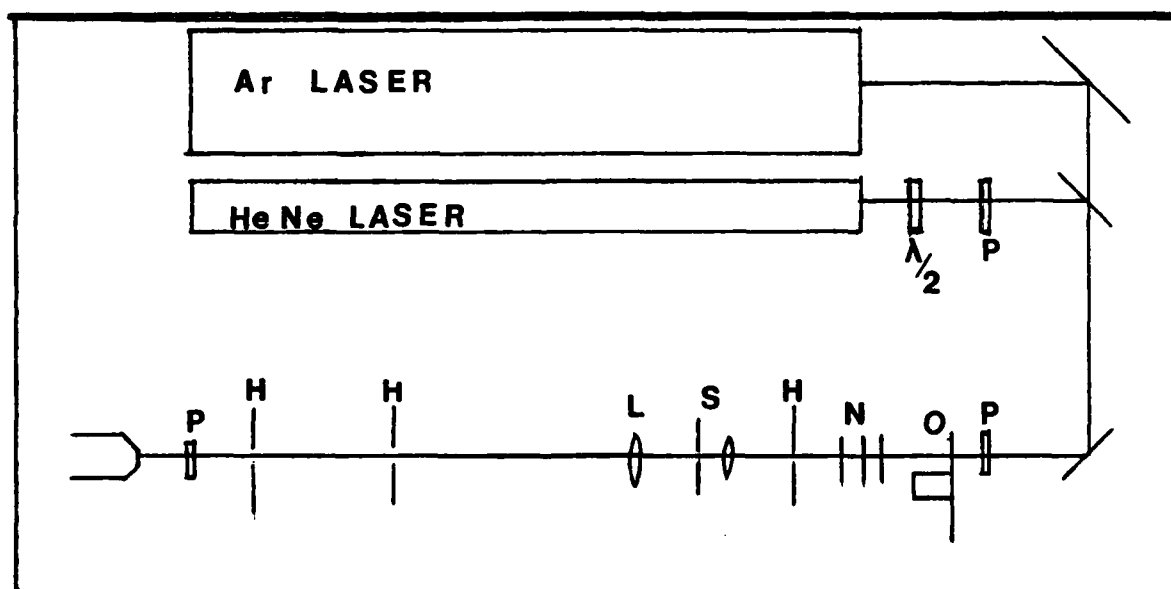
Figure 3.1 The optical system from lasers to fiber optic
light collector. P-polarizers, O-optical chopper,
N-neutral density filters, H-scatter limiting aperture,
S-spatial filter, L-focusing lens.
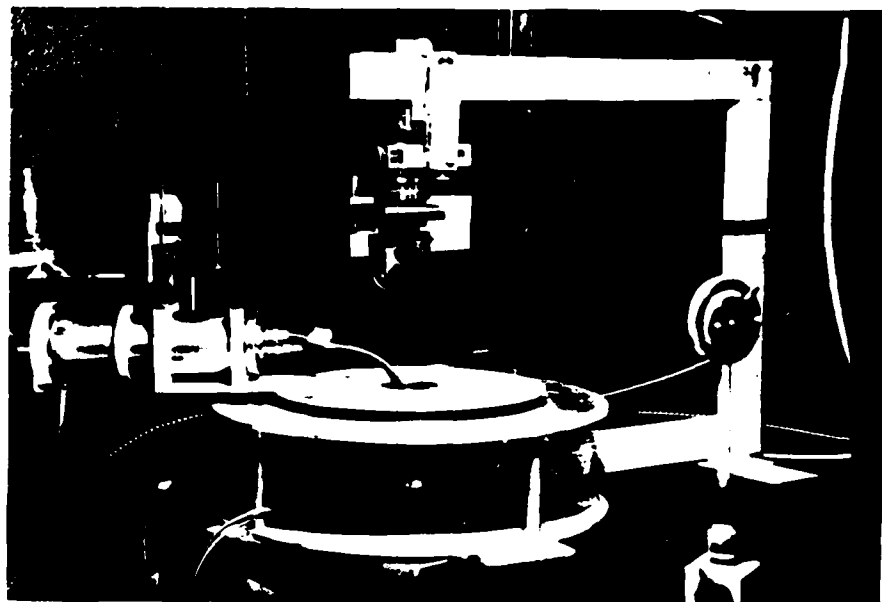
Plate 3.4   Detection system.
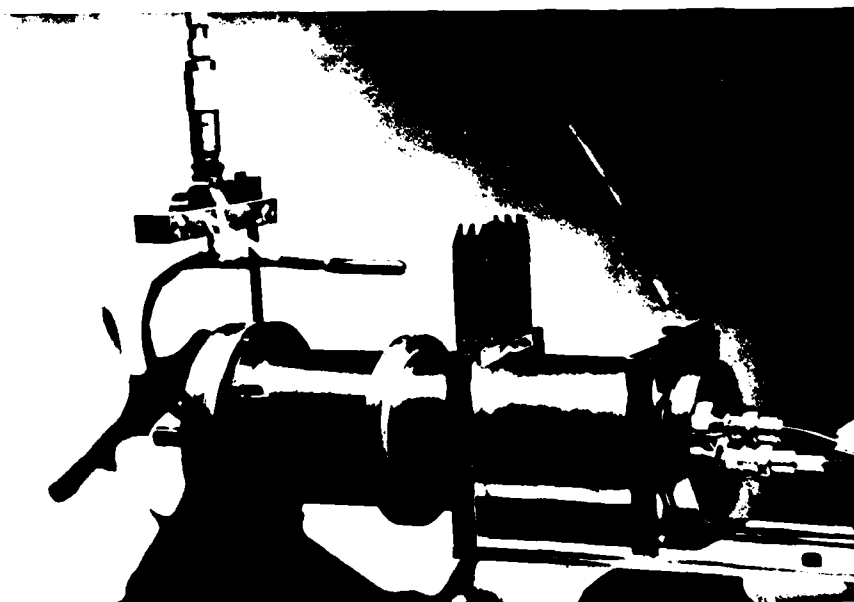
Plate 3.5   Fiber Optic light collector and the photo
multiplier tube.

Figure 3.2   Dimensions of the detector where $\emptyset$ is the diameter and all measurements are made in millimeters.
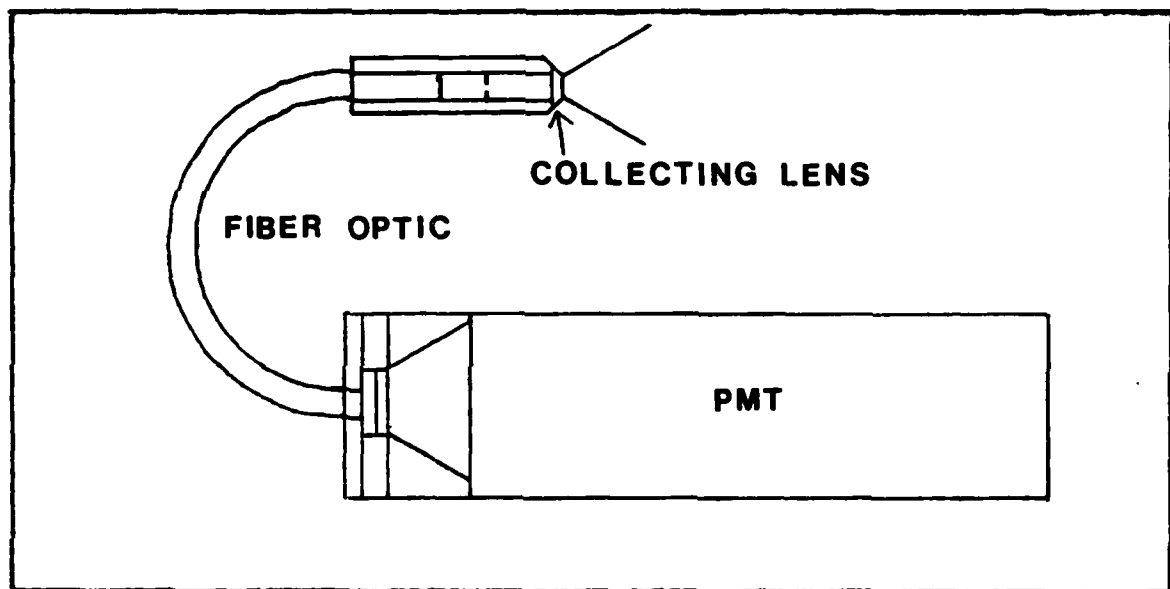
Figure 3.3   The fiber optic light detector.

Plate 3.6   The LSI-11-03 computer.

4.   DATA COLLECTION

In this work the data was collected and analyzed using a computer. The program used for data collection was called SCAT.FOR and was a menu driven control program which provided the following options:

            Initializing the scatterometer control program;
            Measuring system background noise;
            Measuring sample scatter;
            Calculating and displaying PSD curves;
            Calculating and displaying BRDF curves;
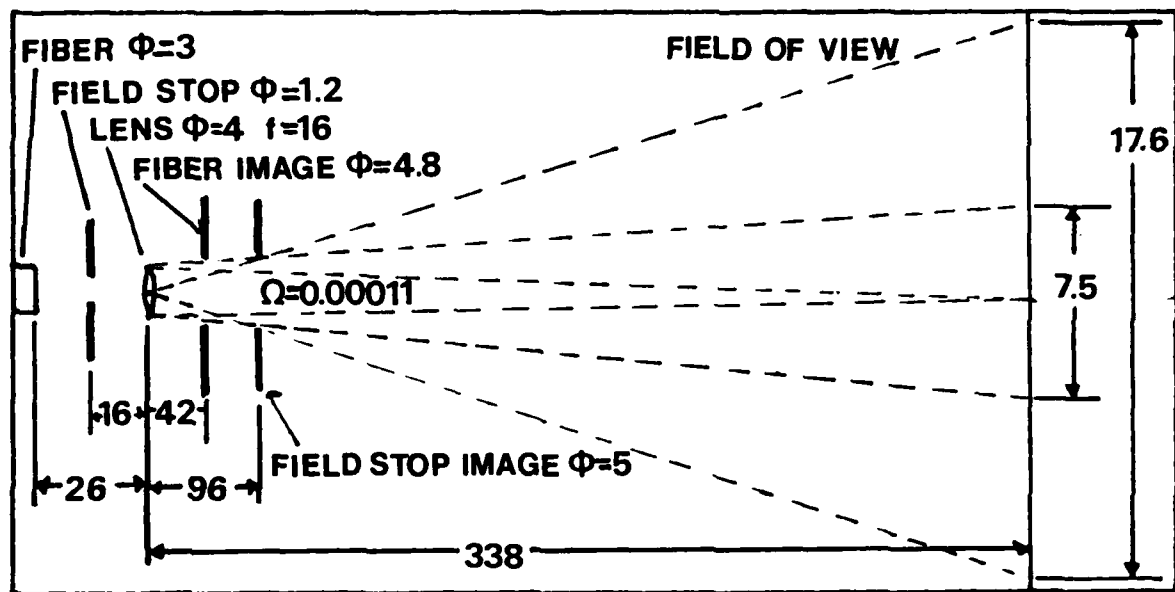   Printing and plotting raw data;
            Testing computer ports.

These options could be requested in any order after the scatterometer control program was initialized, and the system background noise was measured.

4.1   Verification of the PSD and RMS calculations

In order to verify the PSD and RMS roughness calculations, the following procedure was used. A formula to simulate constant scatter intensity which can be used to calculate the RMS roughness is given by:

$$ RMS = \int \int PSD\ d\theta s\ d\phi s \qquad\qquad 4.1\ 1 $$

$$ = \frac{[\ (Is/Ii)\ \tau^4\ (1 \times 10^9)\ 2\pi\ \tan\theta s\ ]^{1/2}}{[.00011\ (16\pi^2)\ \cos\theta i\ ]^{1/2}} \qquad . \qquad 4.1\ 2 $$

A constant voltage signal was applied to the lock-in amplifier to simulate a constant scatter intensity for all angles. The computer then calculated the PSD and RMS

roughness. The results are presented in Chapter 5. These values were then compared to the mathematically calculated value for the RMS roughness.

4.2 Data collection procedure

The following procedure was used to measure the optical scatter data and analyze the results. First, the scatterometer operating conditions were initialized by inputting the number of averages to make for each data point, inputting the range of the scan, inputting the wavelength, setting the sampling interval, and identifying the graphics output device. Second, the system background noise was measured and subsequently accounted for in the calculations.

To measure the scatter, the reflected specular beam must be found. This was accomplished by scanning the detector across the reflected specular beam and recording data every 0.015°. This data provides a profile of the specular beam. To obtain a more accurate value for the intensity of the specular beam, the beam intensity profile data was averaged over the center 0.4°. Then a scatter measurement was made from the center of the specular beam to the specified range. The data at each sampling point consisted of scattered intensity (Is); and scatter angle

(9e). Two sampling intervals were used in data collection. From the center of the specular beam to 0.6° from the center, data was collected every 0.015°; from 0.6° to 90° a sample interval of 0.2° was used. The system background noise was measured, and a PSD and RMS roughness were calculated for the system noise.

A maximum acceptable value for the system background noise was set at 3.0 Angstroms. The system equivalent roughness was never significantly less than 3.0 Angstroms, and this value therefore represented a reasonable standard. If the equivalent system roughness was greater than 3.0 Angstroms, the system was realigned.

Once the system was properly aligned, the sample was placed in the sample holder and adjusted so the detector was in the plane of incidence. The sample was rotated to the desired angle of incidence. A measurement of the scattered light was made in a manner similar to that used for the background system noise measurement.

When scattered light was measured for non-normal incident light, the range of the scan was adjusted so data was not collected for angles greater than 90° from the normal to the sample. This was done automatically by the computer.

4.3   Procedure for depolarization measurement

The scattered light was first measured for the same
polarization as that of the incident light (i.e. SS or PP
polarization). Where the first polarization is the input
light polarization and the second is the collected light
polarization. Then the scattered light was measured with
crossed polarizers (i.e. SP or PS). Depolarization is
defined as the ratio of these two sets of data. SP/SS or
PS/PP. The depolarized light was measured across the
entire front plane of incidence of the surface.

4.4   Data analysis

The PSD curves were displayed by the computer. In
this part of the program the PSD was calculated from the
measured scattered light data, and the RMS roughness was
calculated from the PSD. The spatial frequencies over
which measurements were made were also calculated. The
equations used to make these calculations are:

$$PSD(i) = \tau^4 \frac{Is}{([\Omega \; Ii \; 16\pi^2 \; \cos\theta i \; \cos^2\theta s] \; Q)},$$

4.4 1

$$= \frac{Is \; \tau^4 \; 1\times10^8}{[Ii \; (.00011) \; (16\pi^2) \; \cos\theta i \; \cos^2\theta s \; Q]} . \quad 4.4 \; 2$$

Here Ω is the solid angle of the detector in steradians,

$$Freq(i) = \frac{(\sin\theta s - \sin\theta i)}{\tau},$$

4.4 3

27

$$RMS(i) =$$

$$[freq(i) - freq(i+1)](PSD(i)freq(i)+PSD(i+1)freq(i+1))/2$$
$$4.4.4$$

Note the values were calculated point by point, starting

at the edge of the specular beam, and the units are

Angstroms^2 per microns^{-2}.

Because RMS is an integrated quantity, RMS(i) is the

differential roughness from the edge of the specular beam

to the angle θs. The edge of the specular beam is defined

a. the point at which the scattered light intensity is

twice the system background noise, this is usually .5°.

After calculating these quantities, the computer plots the

PSD versus spatial frequency curves and prints out the RMS

roughness. Also printed are values for spatial frequency

bandwidth of the measurement, the total integrated scatter

calculated from the RMS roughness in ppm, and the amount

of scattered light divided by the amount of specular light

in ppm. This gives accurate numbers for the absolute RMS

surface roughness in a specific spatial frequency

bandwidth.

In the fifth part of the program the bidirectional

reflectance distribution function (BRDF) of the data was

calculated and plotted versus scatter angle. The equation

for BRDF was given by Harvey (11) as

$$BRDF = \frac{I_s}{[I_i \ \Omega \ \cos(\theta_s)]}. \qquad\qquad 4.4$$

Note that BRDF has units of inverse steradians (sr^{-1}).

    There was a second program that was used to analyze depolarization and scatter data called SCTPLO.FOR. See Appendix 2. This program plots SS, SP, PS, PP, SP/SS, or PS/PP versus angle or versus direction cosine. The plots in chapter 5 were made with this program.

5. RESULTS

Measurement of depolarization in scattered light
intensity was performed using an angle-resolved optical
scatterometer. Data is presented here as a result of
examining the effects of angle of incidence, angle of
scatter, film material and surface morphology on intensity
of the depolarized light.

5.1 Verification of PSD and RMS calculations

To verify that the calculation of the PSD and RMS was
correct, the procedure described in Chapter 4 was used.
The results are tabulated in table 5.1. Four test samples
were used with different ratios of Is/Ii. This was done
to insure that the model was correct over the complete
range of sample roughness encountered. The calculated RMS
values were obtained by direct substitution in equation
4.1 2. The correlation between the calculated and
measured values illustrates that the analysis program is
calculating the correct value for the PSD and RMS
roughness. For these calculations, normal incidence was
used. For normal incidence the Q[SS] factor is equivalent
to the reflectance (R[S]) which was set equal to 1.0 for
this test.

A series of tests were also performed to examine the
significance of using the approximated value for Q[SS]
(Q[SS]≈R[S]) instead of the exact expression in equation
2.3 1. A ratio for the correct RMSQ (RMS roughness
including Q[SS]) roughness to the approximation RMS (RMS
roughness with Q[SS] = R[S]) roughness was calculated as a
function of reflectance for various angles of incidence,
and the same shape of PSD curve. Figure 5.4 illustrates
the PSD curves that were used to find the correction
factor curve. This plot illustrates the PSD as a function
of spatial frequency. The values for the correction
factor were found by using different indexes of refraction
in the calculation for the sample PSD curves, and then
averaging the four RMS roughness results. The results are
plotted in figure 5.1. Figure 5.1 illustrates that for
samples with a relatively high reflectance (0.9 ≤ R), the
correction factor is approximately 1.0. Figure 5.1 also
illustrates that the correction factor decreases with
increasing angle of incidence, which indicates that the Q
factor affects the magnitude of the RMS roughness. Figure
5.2 illustrates that the Q factor also affects the shape
of the PSD curve. Figure 5.2 is a plot of the Q factor
versus scatter angle for an incident angle of 2° and for
various materials. This plot illustrates that the Q
factor deemphasizes the high spatial frequency
microroughness and emphasizes the low spatial frequency

31

microroughness, especially for low reflectance films.
Figure 5.3 is a plot of the Q factor versus scatter angle
for an incident angle of 30° and for various materials.
Note that for other PSD curve shapes, the correction
factor curve would be slightly different because the
correction factor is the integration of the PSD curve
including the Q factor.

Very little experimental data involving
depolarization of optical scattered light is presently
available in the literature. Among the data which was
available is that of Bennett (7). Of primary interest in
Bennett's investigation was the amount of retroscatter,
because first order vector scatter theory and experimental
data had the greatest discrepancy for retroscatter. To
match the conditions that were used by Bennett as close as
possible, a glass substrate was coated with silver, and
the retroscatter light intensity was measured. Table 5.2
lists the values for retroscatter ratios for results from
our measurements (UNM) and those of Bennett (NWC).

5.2   PSD results for various samples

Figure 5.4 illustrates the PSD versus spatial
frequency curves for a number of the copper samples
studied. Four samples with roughness ranging from 18 to

95 Angstroms RMS roughness in the spatial frequency
bandwidth from .014 to 1.485 microns^{-1} are plotted.

Figure 5.5 illustrates two PSD curves for two
molybdenum samples. These samples had roughness of 45 and
77 Angstroms RMS roughness. These samples were used in
comparisons with copper samples. The molybdenum is
dominated by low spatial frequency microroughness compared
to the distribution of microroughness of the copper
samples.

5.3   Depolarization as a function of surface
       morphology

Figure 5.6 displays the depolarization for various
copper samples with various RMS roughness and $\theta i = 60°$.
The vertical scale is the ratio of the BRDF of the crossed
polarized light to the BRDF of the light that was in the
same direction as the incident light. The horizontal axis
is direction cosines which were presented by Harvey (11)
and are $\cos(\theta s) - \cos(\theta i)$. By plotting the data using
this method it is centered and symmetric on the plot
making it easier to compare. For some of the plots, the
horizontal extent of the plot is limited because the
amount of scatter for that angle was comparable to the
noise level of the system. Figure 5.6 illustrates the

variation of depolarized light intensity as a function of RMS roughness. Figure 5.7 illustrates depolarization from a sample of copper and a sample of molybdenum with θi = 60°. This depicts the large difference in scatter characteristics of samples having different surface morphologies. The molybdenum has much lower depolarization than the copper. Figure 5.8 illustrates the depolarization for the samples for P input polarized light, and an angle of incidence of 60°. This indicates that the amount of depolarization changes for the molybdenum while it is approximately constant for copper.

5.4 Depolarization as a function of angle of incidence

Figure 5.9 illustrates the variation of depolarization versus direction cosines at several different angles of incidence, for the copper sample with 60 Angstroms of RMS roughness. Depolarization is plotted for θi = 4°, 30°, 60° and 82°. Figure 5.10 illustrates the same sample but with P input polarization and θi = 30°, and 60°. Figure 5.11 illustrates depolarization versus direction cosines from the molybdenum sample with 45 Angstroms of RMS roughness, with θi = 30° and 60°. Figure 5.12 illustrates the depolarization as a function

of angle for the same molybdenum sample with P input polarization. This indicates that for this molybdenum sample, the amount of depolarization depends on angle of incidence.

Table 5.1

Verification of correct calculation of PSD and RMS with constant scatter data.

Is/Ii	Calculated RMS	Measured RMS
$1. \times 10^{-6}$	118.04	118.71
$1. \times 10^{-7}$	38.35	38.62
$1. \times 10^{-8}$	11.88	11.90
$1. \times 10^{-9}$	3.73	3.76

TABLE 5.2

Comparison of UNM retroscattering results to those of Bennett (7) at the Navel Weapons Center (NWC) for 60° angle of incidence on silver samples.

	UNM	NWC	Theoretical
PP/SS	11.9	8.2	40
SP/SS	.114	.215	0 *

* Note that the theoretical value for first order vector scatter theory dose not predict any depolarization in the plane of incidence.
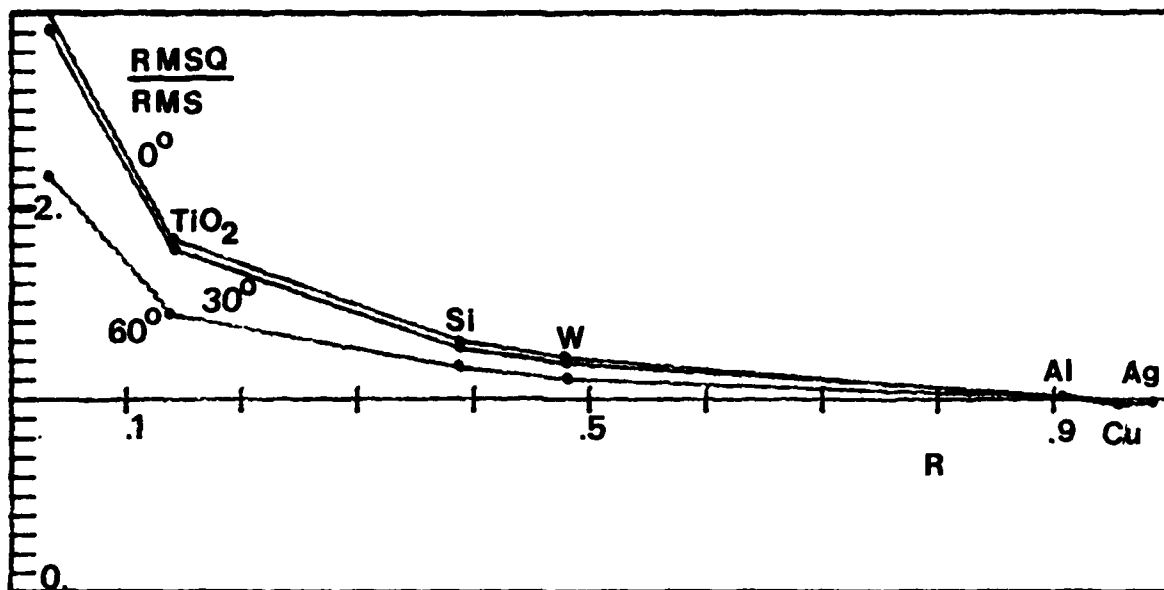
36

Figure 5.1 The correction factor (RMSQ/RMS) versus the
reflectance of the thin film material for near 0°, 30°,
and 60° angle of incidence for the particular PSD
characteristic illustrated in figure 5.4. Note each point
correspond to a different material.

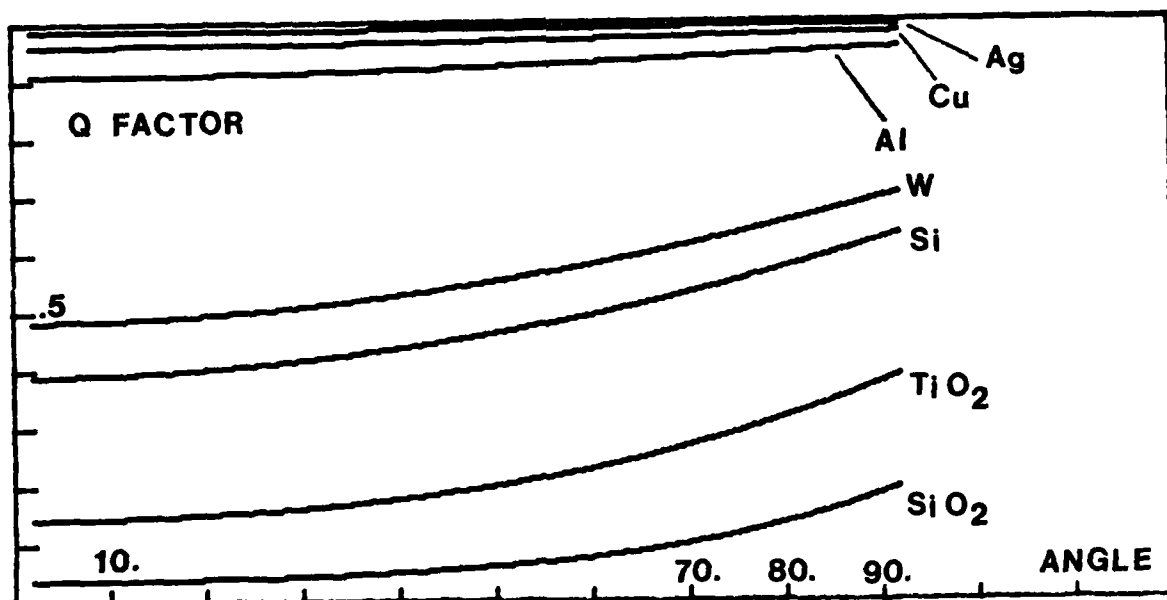Figure 5.2 Q factor versus scatter angle (θs) for an
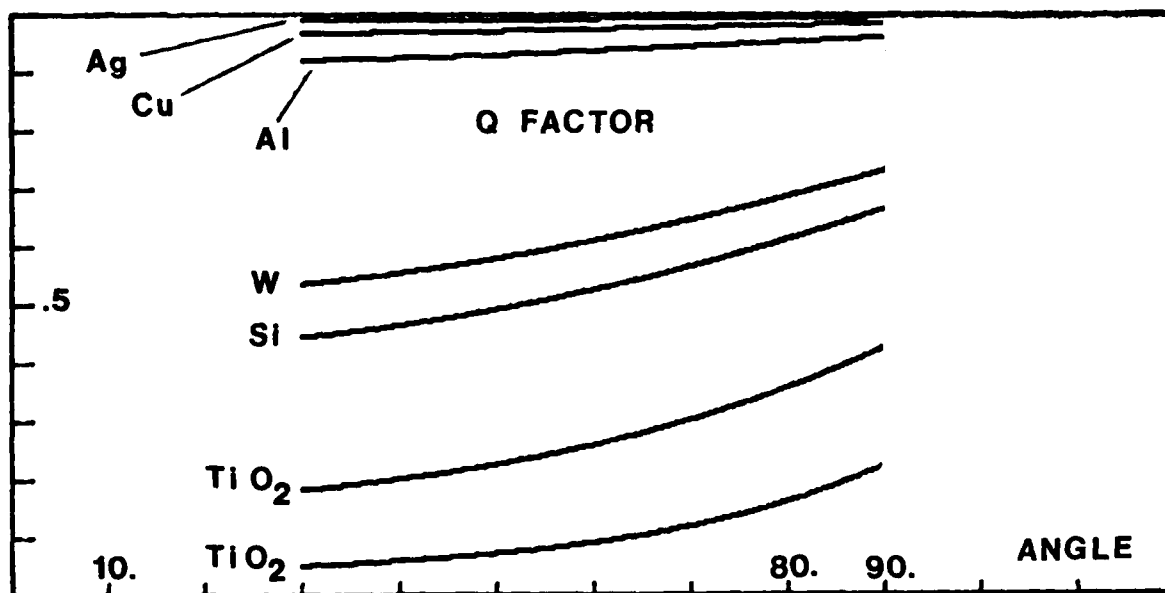incident angel of 2° and various materials.

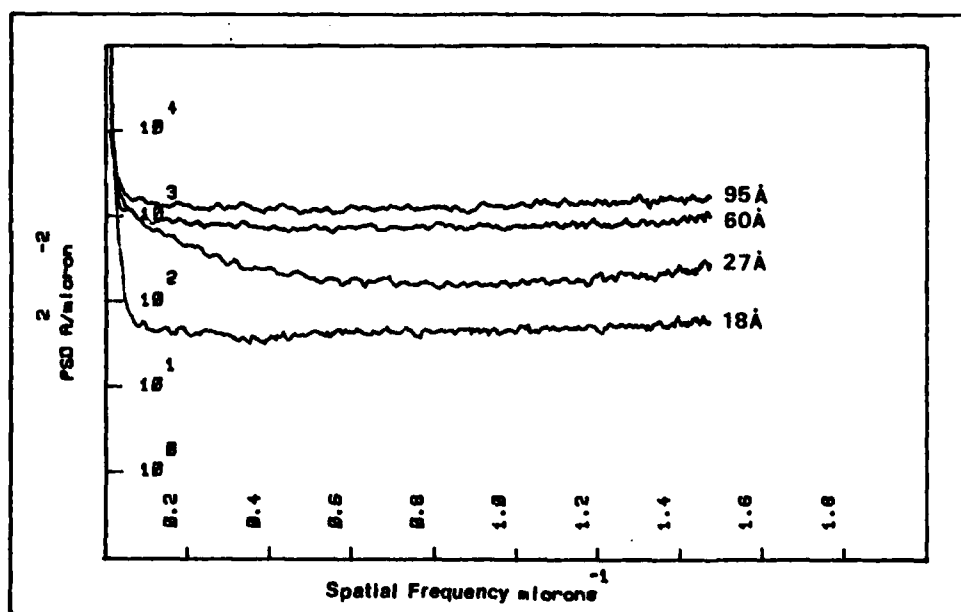Figure 5.3   Q factor versus scatter angle (θs) for an incident angle of 30° and various materials.

Figure 5.4   PSD versus Spatial frequency for copper samples with roughness ranging from 18 to 95 Angstroms RMS roughness, and near normal angle of incidence.
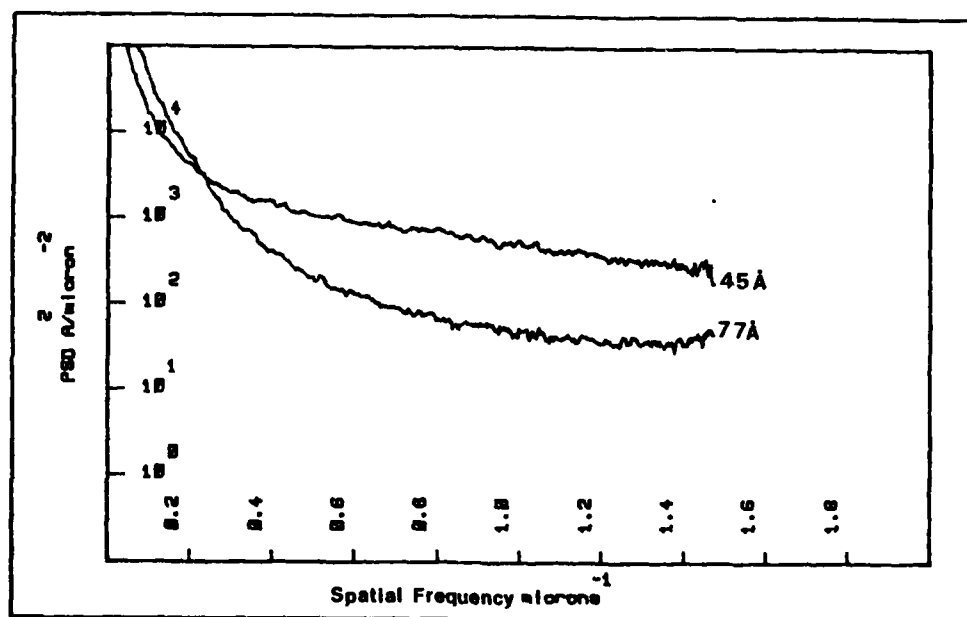
38

Figure 5.5   PSD versus spatial frequency for molybdenum
samples with 45 and 77 Angstroms of RMS roughness, and
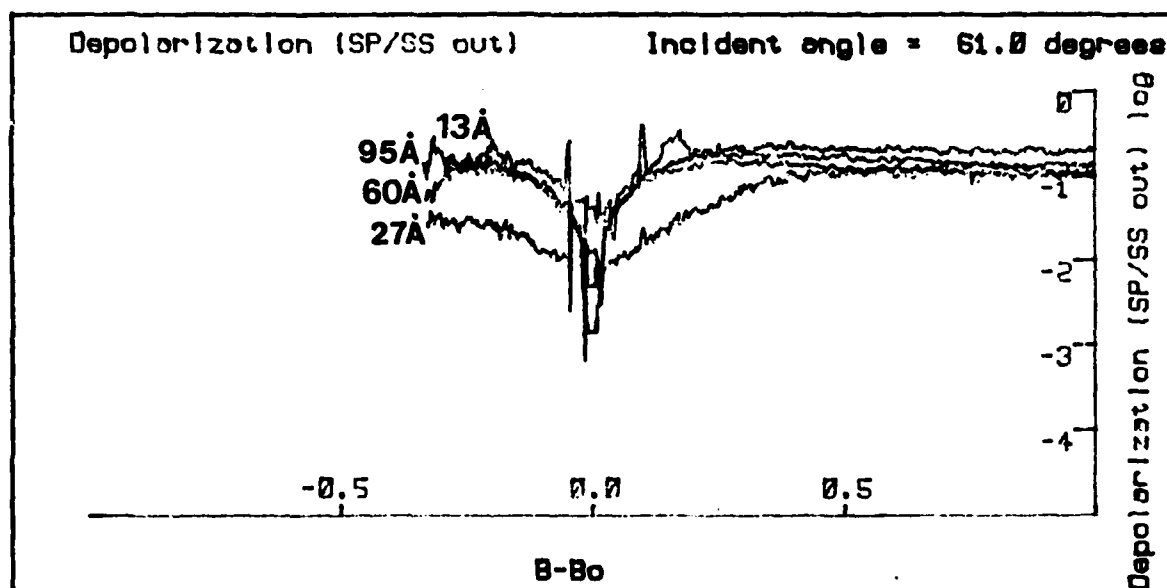near normal angle of incidence.

Figure 5.6   Depolarization versus direction cosines for
copper samples with RMS roughness of 18, 27, 60, 95
Angstroms and $\theta i = 60°$.

Figure 5.7   Depolarization versus direction cosines for
the copper sample with RMS roughness of 60 Angstroms and
for the molybdenum sample with roughness of 77 Angstroms,
and $\theta i = 60°$.
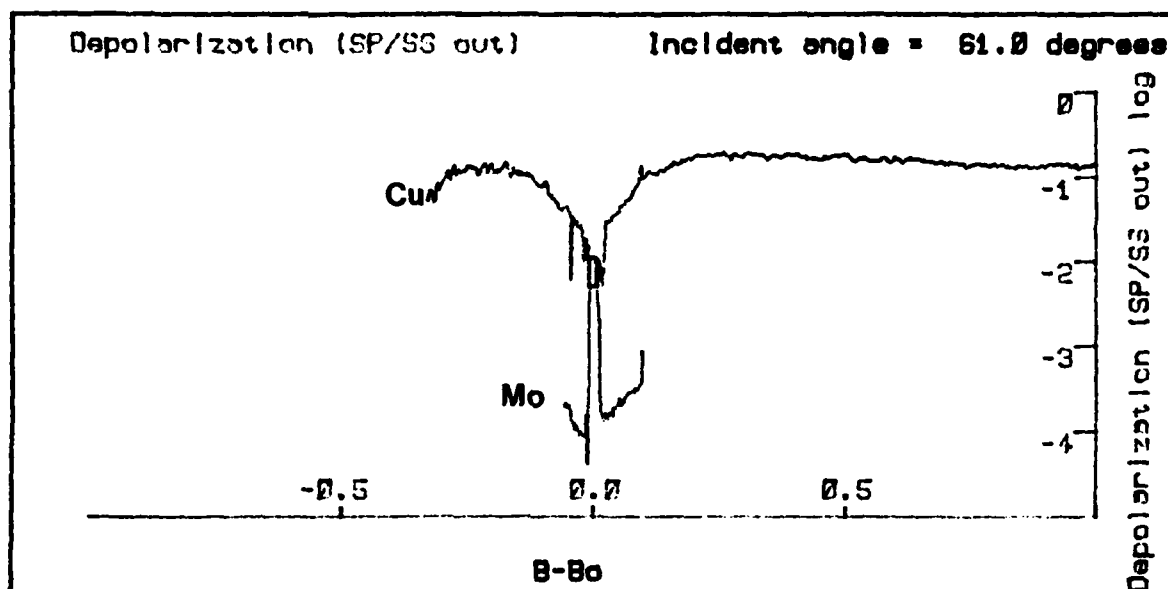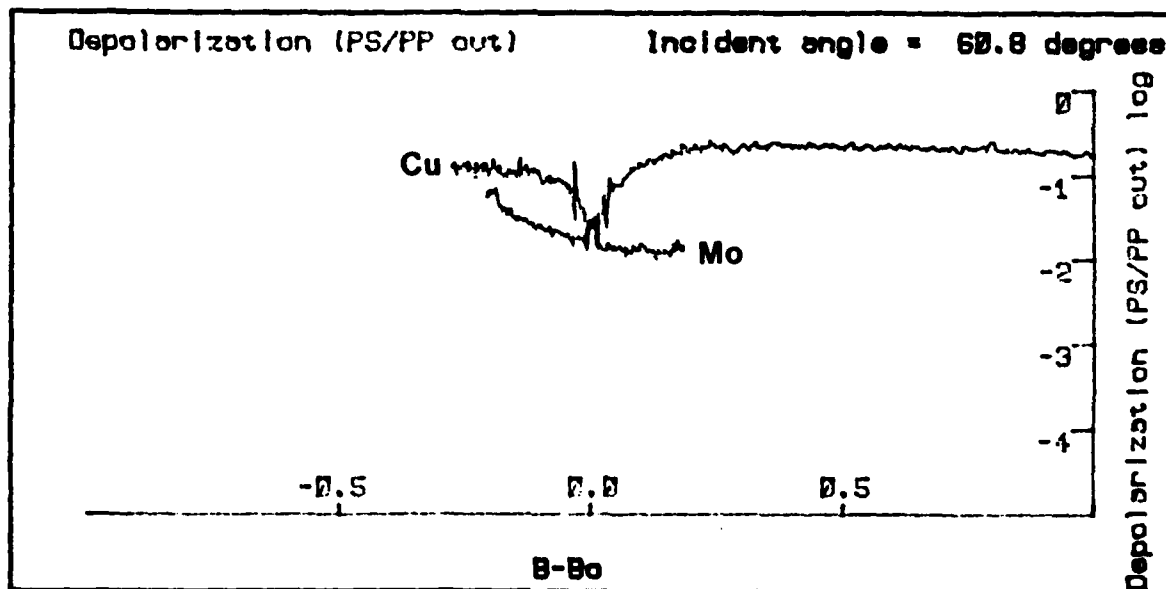

Figure 5.8   Depolarization versus direction cosines for
the copper sample with roughness of 60 Angstroms and for
the molybdenum sample with 77 Angstroms of roughness and
$\theta i = 60°$, with P input polarization.

40
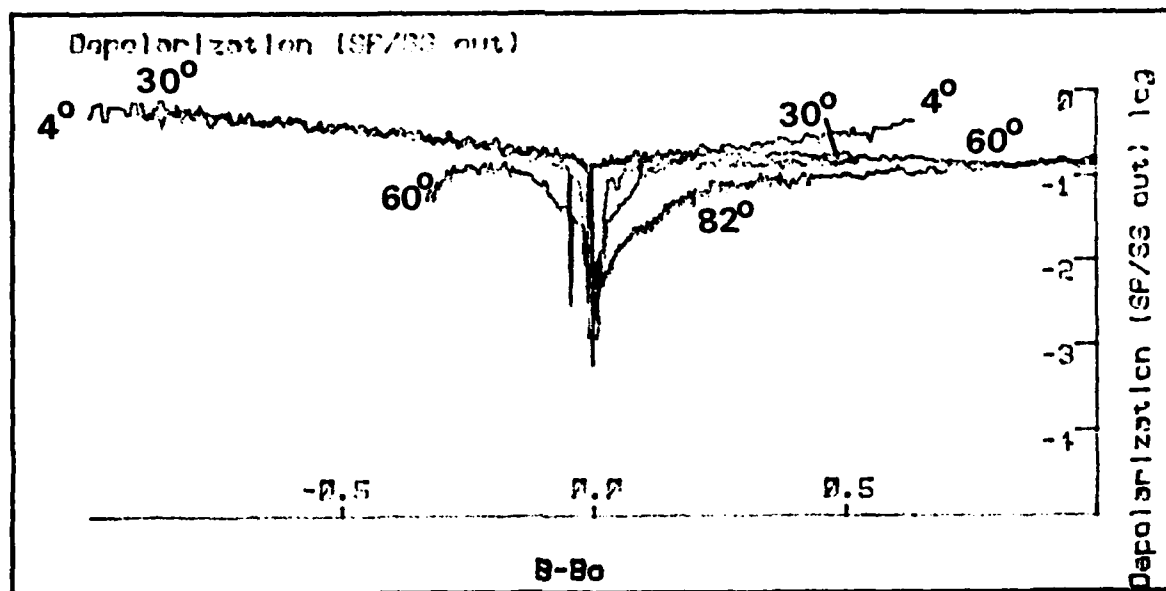
Figure 5.9   Depolarization versus direction cosines for
the copper sample with 60 Angstroms of RMS roughness, and
θi = 4°, 30°, 60°, and 82°.
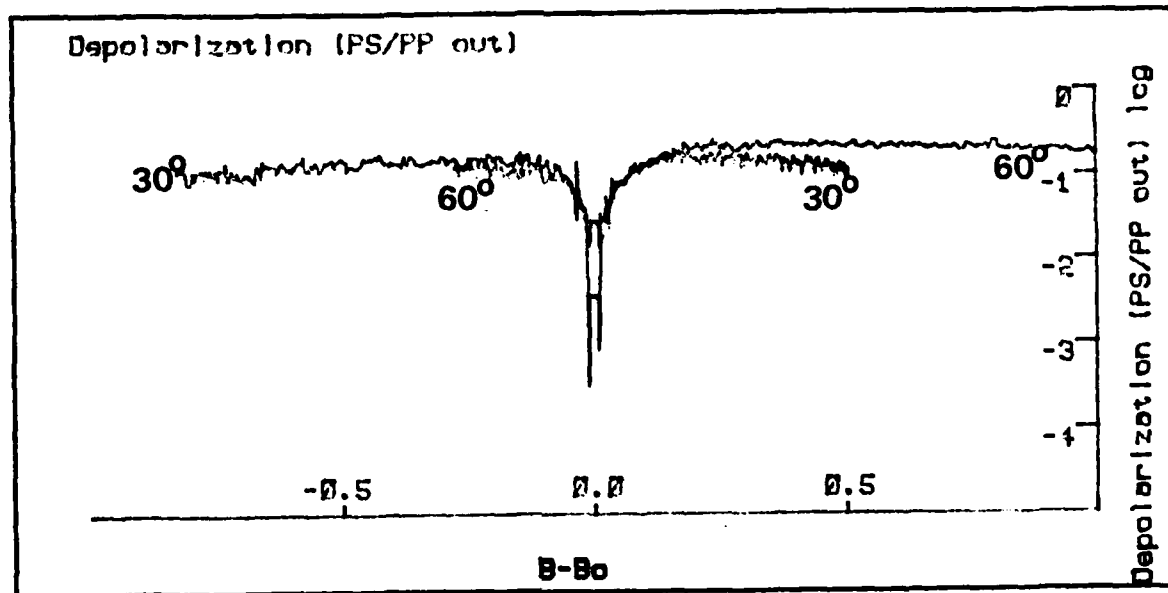
Figure 5.10   Depolarization versus direction cosines for
the copper sample with RMS roughness of 60 Angstroms, and
θi = 30°, and 60°, and P input polarization.

41

Figure 5.11 Depolarization versus direction cosines for
the molybdenum sample with 45 Angstroms of RMS roughness,
and $\theta i = 30°$, and $\theta i = 60°$.

Figure 5.12 Depolarization versus direction cosines for
the molybdenum sample with 45 Angstroms of RMS roughness,
and $\theta i = 30°$, and $60°$, and P input polarization.

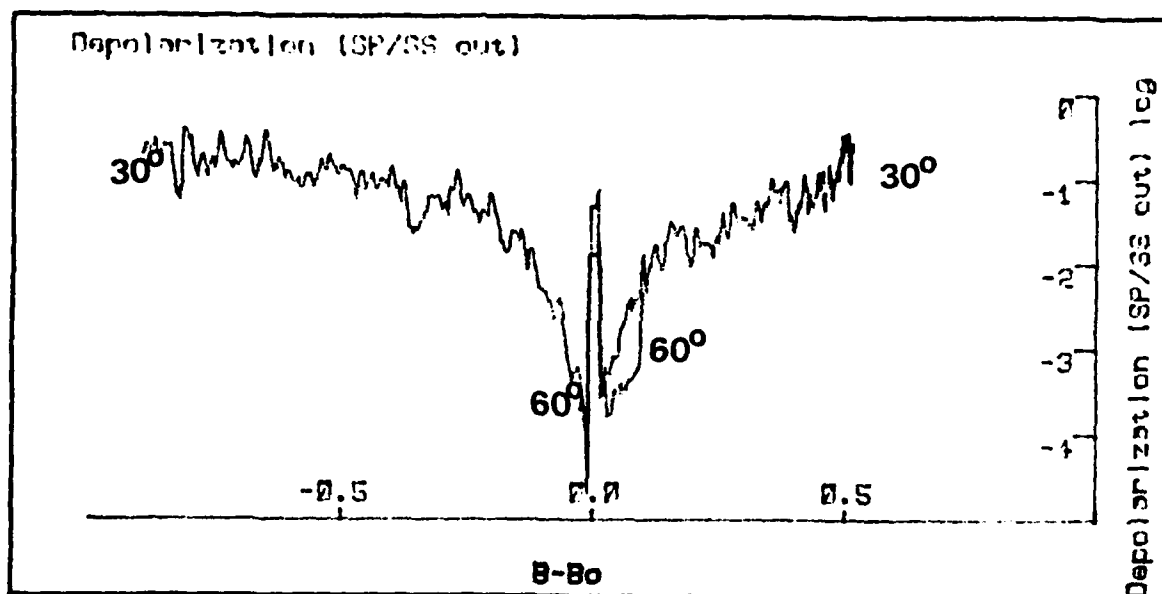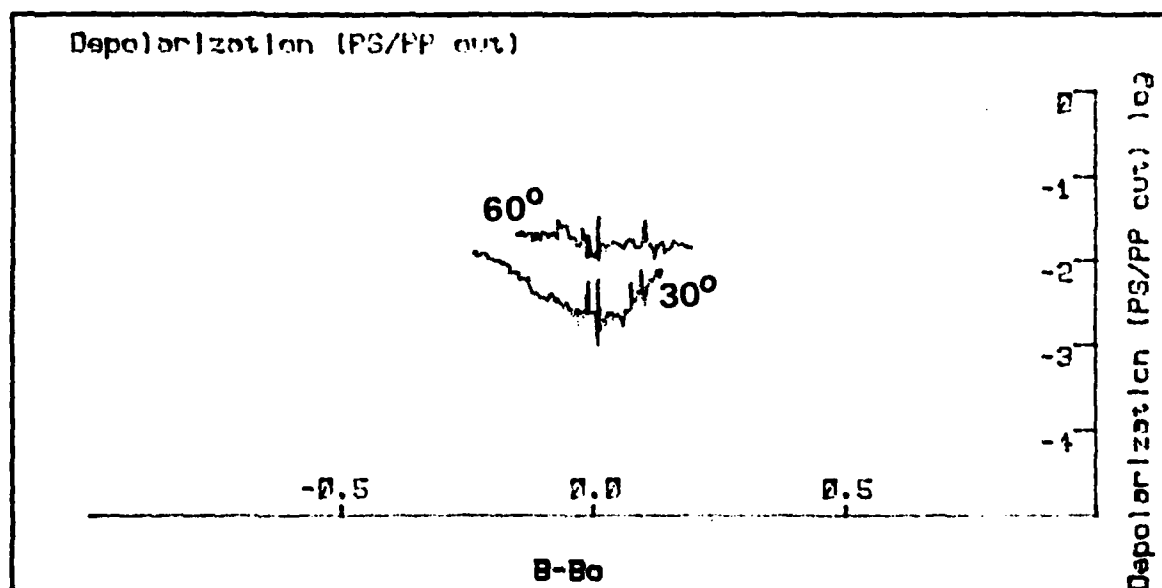# 6. DISCUSSION

In examining the results presented in Chapter 5 it is necessary to discuss how they compare with first order vector scatter theory and Bennett's results.(7)   The results are evaluated to establish what trends, if any, can be found.

In examining the effect of using the exact form for the Q[SS] factor (equation 2.3 1) versus using the approximation (Q[SS]≈R[S]), the following observations can be made.   First, a correction factor RMSQ/RMS can be used to correct the values of the calculated RMS roughness obtained using the approximation for the Q factor. Second, the Q factor changes both the shape and the magnitude of the PSD curve.   The correction factor is different for different materials because the Q factor is a function of optical constants.   In addition the calculated RMS roughness increases when the exact Q factor is used.   This is because the correction factor is greater than 1.   Note that the correction is greatest for samples with low values of reflectance, and that the correction factor is not necessarily the same for different surface morphologies.   The possible difference in the correction factor is due to the integration of the PSD curve which includes the Q factor, over the range of spatial frequencies of observation.   Because of this we have

implemented the Q factor into the calculations instead of using R[S].

Table 5.2 illustrates that the depolarization results measured at UNM are consistent with those reported by Bennett (7) at the Navel Weapons Center (NWC). Both the UNM and the NWC results for PF/SS are significantly lower than the theoretically predicted values. The results from UNM and NWC for depolarization (SP/SS) were comparable. This implies that the measurements made at UNM are consistent with other investigators, and they are lower than the theoretical predictions.

Figure 5.6 illustrates the results of examining depolarization as a function of RMS roughness for a number of copper samples. The RMS roughness for these samples ranged from 18 to 95 Angstroms. It can be seen that the depolarization characteristics for three of the samples are similar, while the sample with RMS roughness of 27 Angstroms is slightly lower for small scatter angles. The data for the copper samples with 18, 60, and 95 Angstroms of RMS roughness have PSD characteristics that are the same shape, and the amount of depolarization is approximately the same for them. For the sample with 27 Angstroms of RMS roughness the shape of the PSD characteristic is different. This indicates that the

distribution of microstructure for this sample is different from that of the other three, and that it is somewhat similar to the PSD characteristics of the molybdenum samples discussed below. This implies that depolarization is caused by the relative amount of high spatial frequency microroughness (i.e. short spatial wavelength) compared to the amount of low spatial frequency microroughness. This might explain the difference in the depolarization characteristics of this sample.

The optical scatter characteristics of two materials were examined; one material (copper) had a relatively higher amount of high spatial frequency microroughness than the other (molybdenum). Figures 5.4 and 5.5 illustrate this by showing typical PSD characteristics for each material. Note that the copper samples were actually Si wavers coated with different amounts of CaF_2 and then overcoated with 2000 Angstroms of evaporated copper. The molybdenum samples were polished from bulk molybdenum.

In order to be thorough, scatter was examined for both input polarizations. Note that for P input polarization, surface plasmons and other effects could influence the scatter. Data is included because of the interesting trends observed that warrant future

investigation. Figure 5.7 illustrates the depolarization
of S polarized light by copper and molybdenum samples.
Figure 5.8 illustrates depolarization for copper and
molybdenum for P polarized light. The amount of
depolarization for the molybdenum sample was much less
than that for the copper sample. This result indicates
that the type of surface microroughness has a large
influence on the amount of depolarization. This further
justifies the proposal above in connection with figure
5.6, that depolarization is caused by the relative amount
of high spatial frequency microroughness compared to the
amount of low spatial frequency microroughness. The
molybdenum surface, on a relative bases has more low
spatial frequency microroughness and less high spatial
frequency microroughness compared to the copper samples
examined.

Depolarization effects were examined as a function of
incident angle for several samples. In the case of copper
samples, depolarization is constant or it decreases
slightly with increasing incident angle, for both input
polarizations for angles far from the specular beam
$(\theta s - \theta i > 30°)$. For angles near the specular beam the
amount of depolarization changed with increaseing incident
angle. Figure 5.9 and 5.10, illustrate depolarization for
a copper sample with various angles of incidence for both

input polarizations as shown. As angle of incidence
increased, the amount of depolarization decreased
symmetrically about the specular beam. This change in
depolarization was not observed for the P input polarized
light. The change in depolarization as a function of
incident angle can not be attributed to shadowing of the
surface morphology because, if it were due to shadowing,
then the depolarization curves would not be symmetrical
for angles near the specular beam ($\theta s - \theta i < 30°$).

In the case of molybdenum samples, depolarization
illustrated a dependence on incident angle for P input
polarization. Figure 5.12 illustrates depolarized
scattered light with P polarized incident light. The
depolarization increases significantly with changes in
incident angle. However, no significant dependence was
observed for S polarized light, which is illustrated in
figure 5.11. These results imply that depolarization is
very dependent on the spatial wavelength of the surface
microroughness, Where as it is not extremely dependent
upon the RMS roughness.

7. CONCLUSIONS

Depolarization from optical surfaces have been examined. The following conclusions can be made:

measurements of retroscatter ratios are comparable with results reported by Bennett (7); results are much lower than the theoretical predictions;

first order vector scatter theory does not predict depolarization in the plane of incidence; experimental data indicates that depolarization is present;

depolarization has little dependence on the RMS roughness of the surface for a specified surface morphology;

depolarization from surfaces with microstructure similar to that of copper is approximately constant with increasing angle of incidence, for both input polarizations;

depolarization from surfaces with relatively more large surface microstructure compared to copper (e.g. molybdenum), increase significantly with increasing angle of incidence for P input polarization, and is approximately constant for S input polarization.

Further investigations could be made in several directions. First, an investigation could be made to examine the results presented above using existing second order vector scatter theory which might explain the occurrence of depolarization in the plane of incidence. Second, a study could be made to extend the findings of this investigation to additional materials to see how the various surface microstructures effect the amount of depolarization. In this investigation the depolarization would be examined as a function of incidence angle to

determine what causes the depolarization to change and be symmetrical for angles near the specular beam. Third, an investigation examining depolarization as a function of light wavelength is warranted. This might provide an understanding of wavelength scaling and how light wavelength effects depolarization. Fourth, an investigation could be preformed to explain the discrepancy between the vector scatter theory and experimental results in the retroscatter ratios.

REFERENCES

1. D.E. Barrick, "Scattering from Surfaces with Different Roughness Scales: Analysis and Interpretation," Battelle Memorial Institute. AD 662 751 (1967).

2. E.L. Church, and J.M. Zavada, "Residual Surface Roughness of Diamond-Turned Optics," Appl. Opt. 14, 1788, (1975).

3. J.C. Stover, "Roughness Characterization of Smooth Machined Surfaces by Light Scattering," Appl. Opt. 14, 1796, (1975).

4. G.R. Valenzuela, "Depolarization of EM Waves by Slightly Rough Surfaces," IEEE Transactions on Antenna and Propagation AP. 15, 552, (1967).

5. S.O. Rice, "Reflection of Electromagnetic Waves from Slightly Rough Surfaces," Comm. Pure. Ap. Math. 4, 351, (1951).

6. F. Jansen, "Investigation of the Surface Roughness of Evaporated Films by Optical Scattering," Ph D. Dissertation Case Western University, Cleveland Ohio, (1977).

7. J.M. Bennett, H.H. Hurt, J.P. Rhan, and J.M. Elson, "Relation Between Optical Scattering, Microstructure, and Topography of Thin Silver Films," Appl. Opt. 24, 2701, (1985).

8. D.E. Barrick. Radar Cross Section Handbook Chap. 9. Plenum Press. Vol. 2 (1970).

9. E.L. Church H. A. Jenkinson and J.M. Zavada, "Relationship Between Surface Scattering and Microtopographic Features," Opt. Eng. 18, 125, (1979).

10. J.M. Elson, and J.M. Bennett, "Vector Scatter Theory," Opt. Eng. 18, 116, (1979).

11. J.E. Harvey, "Light Scattering Characteristics of Optical Surfaces," Phd Dissertation, University of Arizona, Tucson Ariz. (1976).

END

DTIC

9-86